Desalination and Water Treatment
www.deswater.com

doi: 10.5004/dwt.2018.22458

115 (2018) 288–299
May

Fe_3O_4 immobilized magnetic nano carbon balls for the adsorption of methylene blue dye in batch and packed bed column mode

V. Kumaravelan[a], P. Sivakumar[b,*]

[a]*Department of Chemistry, Kandaswami Kandar's College, Velur, Namakkal – 638182, Tamil Nadu, India, Tel. +919442580922, email: vksiniyan@gmail.com (V. Kumaravelan)*
[b]*Department of Chemistry, Arignar Anna Govt Arts College, Namakkal – 637 002, Tamil Nadu, India, Tel. +919865366488, email : shivagobi@yahoo.com (P. Sivakumar)*

Received 26 December 2017; Accepted 6 May 2018

ABSTRACT

Nano sized carbon balls (NCB) with a uniform and average size <100 nm are synthesized from *Madhucalongifolia* oil as a precursor oil using an indigenous reactor assembly through air controlled, low temperature direct pyrolysis with the help of multi-metal catalyst derived from *Alternanthera sessilis* stem ash. The multi-metals present in the stem acts as a green catalyst for the formation of NCB. The synthesized carbon balls have a bulk density of 0.124 g/mL and BET surface area of 805.87 m^2/g. In-order to ensure the effective removal of NCB, it is immobilized with a magnetic nano particle Fe_3O_4 and used for the adsorption studies of methylene blue dye (MB) from aqueous solution under batch and column mode. The batch mode studies indicated that the Fe_3O_4@NCB composite is capable of removing 89.74 mg/g of MB. Batch mode studies also proved the endothermic nature and physisorption mechanisms. The maximum Langmuir mono layer capacity of 277.78 mg/g has been achieved at a temperature of 45°C. A packed bed column study also ascertains the capability of the composite towards the MB removal with a maximum uptake of 118.78 mg/g at an influent concentration of 75 mg/L.

Keywords: Madhucalongifolia; Alternanthera sessilis; Kinetics; Isotherm; Effluent

1. Introduction

The fast growing human population is looking for a comfortable life without compromising the environmental sustainability. The growing populations are aided by the parallel growth of industrial and agricultural sectors. This sort of urbanization, industrialization, developments in science and technology aids the human comfort in the one side and it creates great quantum of pollution on the earth on the other side. Among the different kinds of pollutants discharged on the earth, the pollution levied in the water resources creates a great concern about the life of the flora and fauna. The human health is affected to a great extent due to water contaminants especially in developing countries and under developed countries.

The developed countries are also not too far away from these health issues related to poor quality of water. In this context, it is highly essential to find an affordable technology to remove the contaminants present in the drinking water and industrial wastewater. Numerous technologies have been studied and reported for the wastewater treatment, but all such technologies have some limitations in the form of poor efficiency and high cost involved in implementing the technology to the large scale applications. Among the technologies already reported, adsorption using high surface active materials seems to be a promising technology owing to its selectivity towards wide range of pollutants and its great efficiency [1].

The adsorption using activated charcoal came into practice for about 1000 years back. The adsorption using activated materials for the removal of pollutants in waste-

*Corresponding author.

1944-3994 / 1944-3986 © 2018 Desalination Publications. All rights reserved.

water finds great application even though it is 1000 years old. There are hundreds of materials being tested and reported as an adsorbent for the solute removal. Recently many non-conventional adsorbents like, Potassium hydroxide-treated palm kernel shell [2], brown macro alga [3], nanohydrogel [4] etc have been reported for their capability towards the adsorption of different kind of pollutants.

Recently mono metallic and bimetallic quantum dots based nano composites are also successfully tested for the phytoremediation of textile dyes from wastewater [5]. The main problem associated with these materials is that they have low adsorption efficiency, poor recovery, high manufacturing cost, generation of secondary pollutants during the synthesis of these materials. In such a context, it is highly warranted to prepare an adsorbent from renewable raw materials, low manufacturing cost and energy efficient pathways.

Exploration of materials in the nano scale has great advantages like high surface area, uniform properties, excellent process ability etc. Carbon in nano scale has some exciting morphologies like nanotubes, nano spheres like fullerenes, single layered nano sheets and so on. The nano carbon variants like hollow carbon nano spheres and carbon nano-tubes have been successfully used as composites for hydrogen storage [6], PEM fuel cell cathode [7], adsorptive removal of pollutants [8,9] and super capacitors [10]. It is also used for the remediation of water contaminated with oil [11]. Hollow carbons, bamboo shaped tubes and smooth tubes have been successfully synthesized from benzene, ethylene and acetylene using mixture of metal salt catalysts (Fe, Ni and Co) at high temperature by Kovalevski et al. [12]. During high temperature pyrolysis, the decomposition of precursor oil into a carbon nucleus with solid/liquid & liquid/gas interfaces ends with the radial and concentric texture growth of fluid cokes lead to the formation of nano carbon balls [13]. Synthesis of nano sized carbon materials using biologically renewable precursor or environmentally unimportant materials will certainly be beneficial for the environment as well as the society. The usage of nano carbon materials for the adsorptive removal of pollutants has some limitations like floating on the surface of water and easy leaching with water owing to their small size and low density. In-order to overcome these sort of difficulties, the carbon is immobilized with some magnetically active nano materials like Fe, Ni oxides, which will certainly enhance the recovery of the spent carbon.

The precursor oil for the synthesis of nano sized carbon balls is derived from the plant Madhuca longifolia. It is an Indian tropical tree normally found in the forests of central and north India. It belongs to the family Sapotaceae. A matured tree can produce about 20–200 kg of seeds. The matured dried seeds are used for the extraction of Mahuwa oil. Mahuwa oil with a fatty acid composition of palmitic 24.5%, stearic 22.7%, oleic 37.0%, linoleic 14.3% [14]. The objective of the work is to synthesize highly active nano sized carbon balls (NCB) using *Madhucalongifolia* (Mahuwa) oil with a uniform and average size <100 nm using an indigenous reactor assembly through air controlled, low temperature direct pyrolysis with the help of multi-metal catalyst derived from *Alternanthera sessilis* stem. The synthesized NCB is used for the removal of organic contaminants through adsorption by batch and column mode after immobilizing with Fe_3O_4.

2. Materials and methods

2.1. Materials

All the chemicals used are of analytical grade purchased and used without further purification. All solutions are made using double distilled water.

2.2. Preparation of green catalyst

The muti-metal catalyst has been synthesized from the stems of *Alternanthera sessilis.* The air dried stems of *Alternanthera sessilis* are cut into a pieces of 2–5 cm length and carbonized in muffle furnace at 750°C for 1 h under constant flow 0.1 bar of nitrogen. The carbonized stem pieces are washed twice with double distilled water, followed by a single alcohol wash and finally dried in a hot air oven at 105°C for 24 h [11].

2.3. Synthesis of NCB

The carbonized stems of *Alternanthera sessilis* are soaked with mahuwa oil for about 30 min and then air dried for about 1 h. The air dried, oil soaked stems are kept on a stainless steel grill and it is burnt from the bottom using LPG gas as a fuel mixed with air as shown in Fig. 1. The soaked stems start to burn at its ignition temperature, then the fuel gas (LPG) is cut off and the air inlet is regulated in such a way that, the combustion temperature is controlled at 420–470°C. The soot formed during the combustion is collected using a dome shaped surface of chromium oxide layer of stainless steel lid (316SS) which is kept over the combustion chamber. The excess flue gas is allowed to pass through the exhaust vents. The ash formed during the combustion process is frequently removed through the discharge opening provided at the bottom of the reactor. The carbon deposited at the inner surface of stainless steel dome is carefully collected and washed with double distilled water and finally with alcohol.

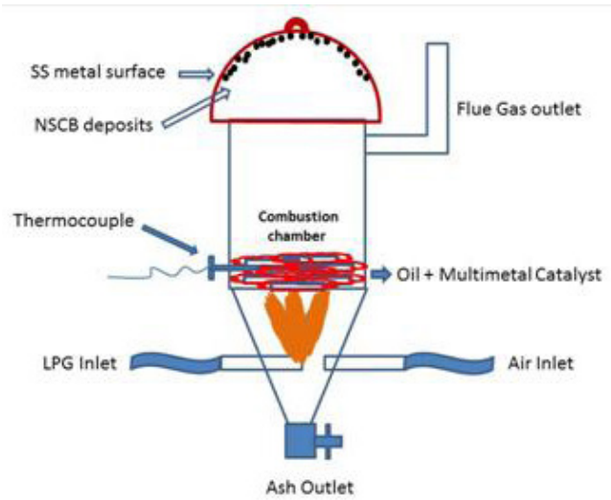

Fig. 1. CVD reactor assembly for the synthesis of NCB.

2.4. Activation of NCB using microwave oven

The carbon balls collected in the above process are stirred with minimum quantity of 4 N nitric acid and made into a paste. The paste is kept in microwave oven and activated at 600 W for 5 min. Finally the activated NCB is washed with double distilled water 4 times and an alcohol wash, then dried in a hot air oven for 2 h at 105°C and finally used for further studies.

2.5. Synthesis of iron oxide immobilized NCB (Fe_3O_4@NCB)

Exactly 100 ml of 0.1 M solution of $FeCl_3 \cdot 6H_2O$ is mixed with 0.5 g of activated NCB and stirred with magnetic stirrer for about 30 min. Then 1:1 ammonia is added drop wise with this mixture with constant stirring. The gel formation takes place at a pH of 8.0. After the gel formation, the ammonia addition is stopped and the contents are continuously stirred for another 4 h. After 4 h, the carbon immobilized with Fe is carefully filtered, washed, dried in hot air oven at 110°C for 24 h and then finally calcined at 400°C for 1 h under constant flow of nitrogen at 0.1 bar. The calcined Fe_3O_4@NCB magnetic composite is cooled to room temperature and stored in tight lid container for further studies.

2.6. Characterization

The surface morphology is examined using field emission scanning electron microscope (FE-SEM) ZEISS (Saint Joseph College, Trichy, India) at an accelerating voltage of 5 kV. The NCB and the composite nano particles are characterized by powder X-ray diffraction (PAN alytical X'Pert PRO powder X-ray Diffractometer, Alagappa University, Karaikudi, India) equipped with Cu-Kα (l = 1.54 Å, 40 kV, 30 mA, 40 kV and step width 0.05 degree). The XRD of the composite is recorded for a 2θ range of 10.02 to 80.92° with a scan step time of 10.16 s. TGA studies performed at a heating rate of 20 K/min up to 900°C with NETZSCH instrument model STA 449F3 Jupiter.

2.7. Batch adsorption studies

Methylene blue (MB), dye (basic dye) with a molecular weight of 319, formula $C_{16}H_{18}ClN_3S \cdot 2H_2O$, C.I No. 52015 and the absorption maxima at 665 nm, (E. Merck, India) is used as a model solute for the adsorption studies. A stock solution of 1000 mg/L is prepared using appropriate amount of dye dissolved in double distilled water and diluted as and when required. For the batch mode adsorption studies, 100 mL of dye solution of specified concentration is equilibrated with 100 mg of Fe_3O_4@NCB composite in 250 mL tight lid reagent bottle (Borosil-R glass bottles) using REMI make orbital shaker. For the effect of pH, 1 M HCl and 1 M NaOH solutions are used to adjust the pH of the solution. After the specified time of agitation, the contents of the flask are centrifuged using universal make centrifuge at 5000 rpm and the final concentration of the dye solution is estimated by measuring the absorbance at the λ_{max} of the dye solution (665 nm) using UV-VIS spectrometer(Model : Elico-BL198). All the adsorption experiments have been done in duplicated and the maximum deviations from the two runs are 4% only.

The percentage and amount of dye removed through adsorption is calculated using the following relationships.

$$\text{Percentage of dye removed} = \frac{Intial\ concentration(C_0) - Concentration\ at\ time\ t(C_t)}{Initial\ concentration(C_0)} \times 100 \quad (1)$$

Amount of dye removed per unit weight of adsorbent $(q_t) = (C_0 - C_t)\frac{V}{W} mg/g$ (2)

where V is the volume of dye solution in mL and W is the weight of adsorbent in grams

2.8. Column adsorption studies

Large scale industrial operations require the evaluation of any new adsorbent to be tried in column mode also. The fixed bed reactor is designed in laboratory scale using glass column of 1.2 cm diameter and 40 cm height. The adsorbent is packed over a porous silica dick kept at the bottom of the column and the top is covered with glass wool. The dye solution is fed from the bottom using a peristaltic pump in an up flow method in-order to ensure proper contact between the solute and sorbent. The treated solution coming out of the column is analyzed for the residual dye concentration using UV-VIS spectrometer (Model: Elico-BL198) as stated above.

2.9. Error analysis

The adsorption capacity obtained by the various mathematical models is compared with that of the experimental adsorption capacity using the following Error analysis method.

$$Sd = \sqrt{\sum \frac{(q_{0(\exp)} - q_{0(cal)})^2}{N}} \quad (3)$$

where $q_{0(exp)}$ is experimental adsorption capacity, $q_{0(cal)}$ is the adsorption capacity calculated using theoretical kinetic models and N is the number of experimental points run.

3. Results and discussion

3.1. Surface characteristics of the NCB and Fe_3O_4@NCB

During the combustion of Mahuwa oil, nano sized carbon balls are deposited at bottom surface of the SS dome. The synthesized carbon is washed with distilled water and the surface topography is tested using SEM images. The SEM images (Fig. 2a) of pure carbon indicated that the nano carbon balls with extremely uniform size of 40 to 80 nm are formed. The SEM images of the Fe immobilized on NCB (Fe_3O_4@NCB) is shown in Fig 2b. There is a uniform distribution of Fe_3O_4 on the surface of carbon without much agglomeration. The Fig. 2c is the SEM image observed after adsorption, which clearly indicate the uniform distribution of dye molecules over the surface of Fe_3O_4@NCB. All the NCB are of spherical and uniform in size. The smaller size

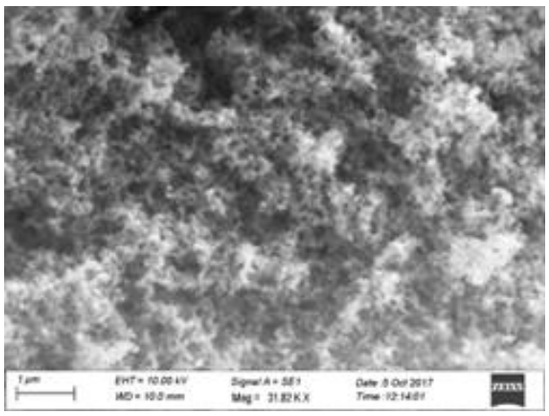

(a)

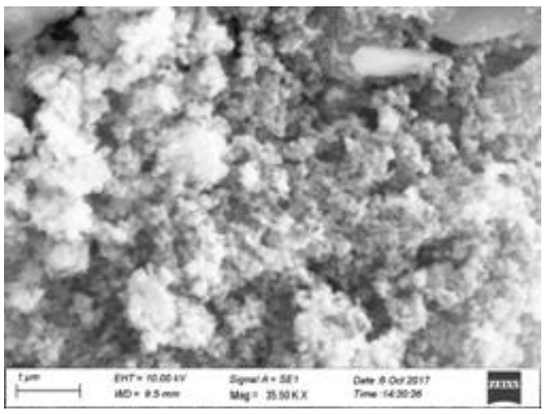

(b)

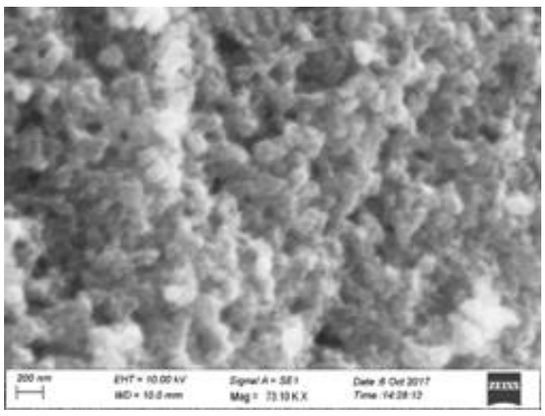

(c)

Fig. 2. SEM images a) NCB b) Fe_3O_4@NCB c) Fe_3O_4@NCB after adsorption.

nano carbon balls give large surface area as indicated from the BET surface area analysis studies (Table 1). The immobilization of Fe slightly reduces the total surface area, where as this can be compromised with other advantages like, increased bulk density and magnetic behavior. The lower bulk density values given in Table 2 indicate that, the synthesized carbon balls are very small in size with some hollowness inside the balls. This lower density also indicates the high surface to bilk volume of the synthesized NCB.

Table 1
Physico-chemical properties of NCB and Fe_3O_4@NCB

S.No	Property	NCB	Fe_3O_4@NCB
1.	pH	6.9	7.4
2.	pH_{ZPC}	6.6	7.1
3.	Bulk Density, g/mL	0.124	0.221
4.	BET Surface Area, m^2/g	805.87	774.08
5.	Moisture content, %	8.71	9.12
6.	Volatile matter, %	3.34	3.26

Table 2
Comparison of bulk density values of carbonaceous materials

S.No	Sample	Bulk density g/mL	Reference
1.	Graphite	2.22	[15]
2.	Multi walled carbon nano tubes	1.74 ± 0.16	[15]
3.	Solid carbon nano spheres	1.66	[16]
4.	Nano carbon hollow spheres	0.025	[11]
5.	Uniform mesoporous carbon spheres	0.762	[17]
6.	Mesoporous activated carbon from Euphorbia antiquorum L	0.48	[18]
7.	NCB	0.124	Present study
8.	Fe_3O_4@NCB	0.181	Present study

The XRD pattern of NCB and composite are shown in Fig. 3a. This plot has a broad pattern at 25°,which is generated due to the reflections of (002) graphitic plane. This is a typical pattern of amorphous structure with a d_{002} of 0.036 nm, which is calculated based on Bragg's equation (JCPDS 41–1487). This gives a quantitative measurement for the graphitic network [19]. Presence of another peak with low intensity observed around 44° generated by the reflection of (100) graphitic plane [20]. The immobilization of Fe_3O_4 on the graphitic layer does not show much influence of d_{200} spacing as indicated by the position of XRD peak at 25.0° (which does not have any shift in Fe_3O_4@NCB). The characteristic peaks for Fe_3O_4in Fe_3O_4@NCB composite are observed at a 2θ angles of 18.0, 30.0, 35.5, 37.0, 43.5, 53.0, 63.0 and 71.5° corresponding to the (111), (220), (311), (222), (400), (422), (511), (440) and (620) planes respectively (JCPDS card No. 19–0629) [21]. The TGA curves in Fig. 3b indicated that the combustion started around 500°C and completed around 630°C. This high temperature combustion substantiate the presence of graphitic layers in the NCB [22].

3.2. Formation and growth mechanism of NCB

In our previous work we have evaluated the elemental composition of multi-metal catalyst, which contains metals

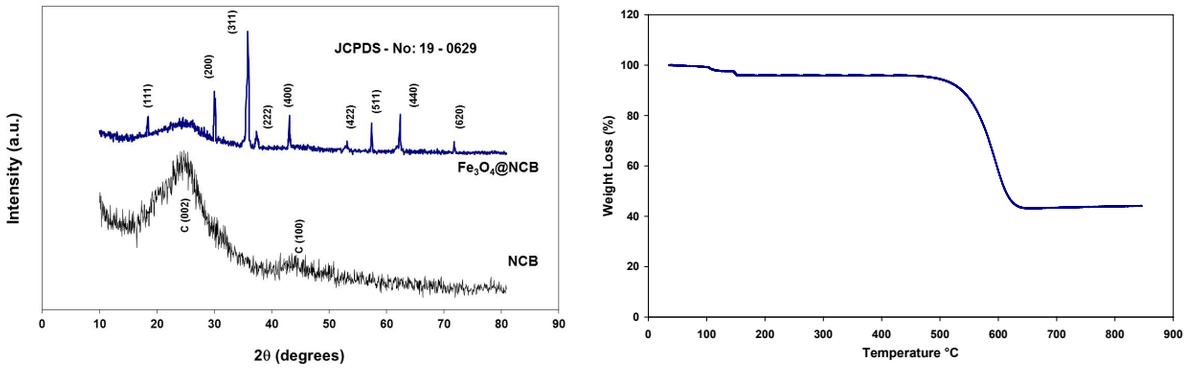

(a) (b)

Fig. 3. (a) XRD pattern of NCB and Fe_3O_4@NCB composite, (b) TGA curve of NCB.

such as Al, Fe, Ni and Cu with the concentrations of 47, 34, 1.4 and 0.6 g/kg on dry matter basis respectively [11]. As reported from Kim et al. [23], during the combustion, the metals form alloys, the Cu-Ni alloy has a capability of 100 times faster gasification of the precursor oil than the Ni metal. Similarly, the other metals also form variety of alloys at the combustion temperature, which favours the gasification of the precursor. The gasified precursor burns at the surface of catalyst at lower temperature [24]. The controlled combustion of the precursor oil at lower temperature and sort supply of oxygen leads to the formation of carbon bubbles at the surface of nano multi-metal catalyst surface. These bubbles fly upward and reach the cold surface of dome shaped SS catalyst surface and get stuck on its surface. As the temperature of the surface is very low when compared with that of combustion chamber, the growth of bamboo like carbon nano tube (CNT's) formation is prevented. Instead of forming the CNT's, at the colder surface, the carbon balls forms strings of nano carbon balls as shown in Fig. 4.

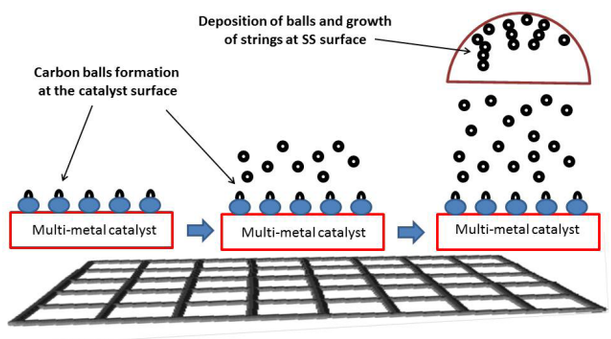

Fig. 4. Mechanism of NCB formation.

3.3. Dye adsorption studies

The synthesized Fe_3O_4@NCB is evaluated for its capability towards the adsorptive removal the selected basic dye (methylene blue) under batch and column mode. Initially batch adsorption studies are conducted to evaluate the effect of solution pH, initial dye concentration and temperature. The change in thermodynamic parameters during the adsorption is also investigated by studying the isotherm parameters at different temperatures. The large scale industrial operations require the evaluation of the selected adsorbent-adsorbate system under column mode operations. The subsequent sections deal with the evaluation various controlling factors, kinetics, isotherms and thermodynamics of the Fe_3O_4@NCB-MB adsorption system.

3.4. Batch mode adsorption studies

3.4.1. Effect of pH

Any adsorption systems involving either physical forces or chemical forces of attraction are greatly influenced by the solution pH as well as the surface charges present on the sorbent surface. The effect of solution pH on the adsorption of MB by Fe_3O_4@NCB is studied by varying the solution pH from 2.0 to 12.0 as shown in Fig. 5a. On increasing the solution pH from 2.0 to 6.0, the uptake of MB dye shows a slight increase. When the pH goes beyond 6.0, the adsorption of MB increases to a large extent upto a pH of 9.0 and then finally the pH exceeds 9.0, there is no much changes in the extent of MB adsorption. In aqueous solution, the basic (cationic dye) MB exist as $[MB]^+$ and $[Cl]^-$. When the pH is lower than the pH_{ZPC} of adsorbent, the adsorbent exist as protonated (the pH_{ZPC} of Fe_3O_4@NCB is 7.1), the protonated Fe_3O_4@NCB surface repel the positively charged cationic dye species and the amount of MB removed is low at pH lower than the pH_{ZPC} of Fe_3O_4@NCB. The maximum removal of MB by Fe_3O_4@NCB achieved at a pH of 8.0 is 96.5% for an initial MB concentration of 50 mg/L. The dynamics and mechanism of the variation adsorption with respect to pH is represented in Fig. 5b.

The effect of pH on desorption of MB from the dye loaded adsorbent is also shown in Fig. 5a. For the desorption studies, a fixed quantity of dye loaded adsorbent is agitated with distilled water having dil HCl or 0.1 N NaOH (to attain a specific pH). The solution is centrifuged and then analyzed for the residual MB concentration as stated above. Maximum desorption is achieved at a pH of 2.0. The cat-

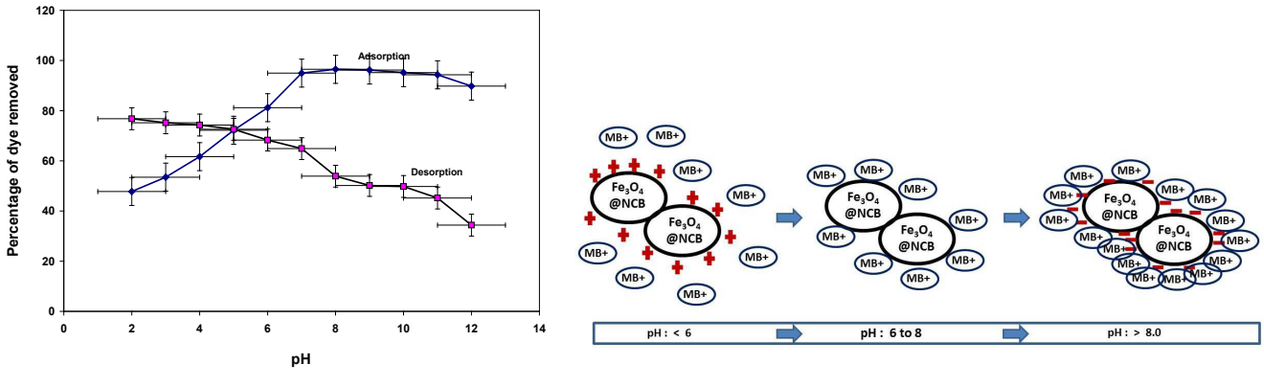

(a) (b)

Fig. 5. (a) Variation of MB Adsorption at various pH, (b) Mechanism of MB Adsorption onto Fe_3O_4@NCB surface at various pH.

ionic dyes are easily removed by the competitive protons at lower pH. At higher pH, the hydroxyl ions are not capable to desorb the dyes like protons. Distilled water with lower pH is a suitable eluent for the desorption of MB dye from Fe_3O_4@NCB surface.

3.4.2. Effect of initial dye concentration

Lab scale evaluation has great influence over the adsorption of a solute by a sorbent. It is highly essential to evaluate the effect of initial MB concentration in-order to optimize the other influencing parameters. The effect of initial MB concentration is evaluated by varying the initial dye concentration from 25 to 100 m/L for a fixed volume of 100 mL with a dosage of 100 mg. The variation of adsorption with respect to concentration is graphically represented in the Fig. 6a. As observed from the figure, the amount of MB removed at equilibrium is increased from 25.0 to 89.74 mg/L when the concentration is increased from 20 to 100 mg/L. During the beginning and the initial phase of adsorption, the rate of adsorption is very fast due to the availability of more adsorption sites as well as higher number of active sites per unit quantity of solute [25]. On progression of adsorption, the ratio of available sites per unit quantity of solute decreases, which ultimately reduces the rate of adsorption. After 90 min of contact time, the adsorption/desorption reached an equilibrium and practically there is no change in the concentration of solute in the liquid phase. Based on these results, the equilibrium contact time for isotherm studies fixed as 120 min. At equilibrium the maximum quantity of MB removed per gram of Fe_3O_4@NCB increased from 25.0 to 89.74 mg/g on increasing the initial MB concentration from 25 to 100 mg/L. The profile indicated that the adsorption follows Type-I Langmuir type of isotherm, the sorbent surface gets saturated with one layer thick of MB. The size of NCB is only fewer times larger than the size of solute molecule, therefore, further multilayer adsorption is not possible [26].

3.4.3. Effect of temperature

Effect of temperature is studied by varying the solution temperature from 30 to 45°C at an initial MB concentration of 50 mg/L as shown in Fig.6b. Generally heat evolved (exothermic) if the adsorption is physisorption [27]. The results of MB adsorption onto Fe_3O_4@NCB composite show a decreasing trend on increasing the temperature from 30 to 45°C. The NCB surface is smooth and the surface to bulk volume is high (due to the nano sized NCB) which results in binding the solute molecules through weak Vander waals forces of attraction. The MB uptake by Fe_3O_4@NCB composite is decreased from 48.78 to 45.12 mg/g on increasing the temperature from 30 to 45°C. When the temperature of the system is elevated, normally the kinetic energy of the solute molecules increases, and there by the weak bonding between the sorbent surface and the solute is ruptured. The breaking of bonding between MB and NCB is proportionally increases with increase of temperature, ultimately the quantity of solute present on the sorbent surface decreases. Many authors have reported the swelling of adsorbent surface favors the more uptake of solute [28], whereas in this case, the desorption caused by the increased kinetic energy dominates and thereby the adsorption show a decreasing trend with respect to increase of temperature.

3.5. Kinetics of adsorption

In-order to evaluate the kinetics of adsorption and also to reveal the mechanistic evidence for the adsorption of MB by Fe_3O_4@NCB composite, the kinetics models like pseudo-first order model [29], pseudo-second order model [30], and intra-particle diffusion model [31] are used. The linear form of these kinetics models are:

Pseudo-first order model: $$\log(q_e - q_t) = \log q_e - \frac{k_1}{2.303}t \quad (4)$$

Pseudo-second order model: $$\frac{t}{q_t} = \frac{1}{k_2 q_e^2} + \frac{1}{q_e}t \quad (5)$$

Intra-particle diffusion model: $$q_t = k_d \cdot t^{1/2} \quad (6)$$

where q_e is the amount of dye adsorbed at equilibrium (mg/g), q_t is the amount of dye adsorbed at time 't' (mg/g),

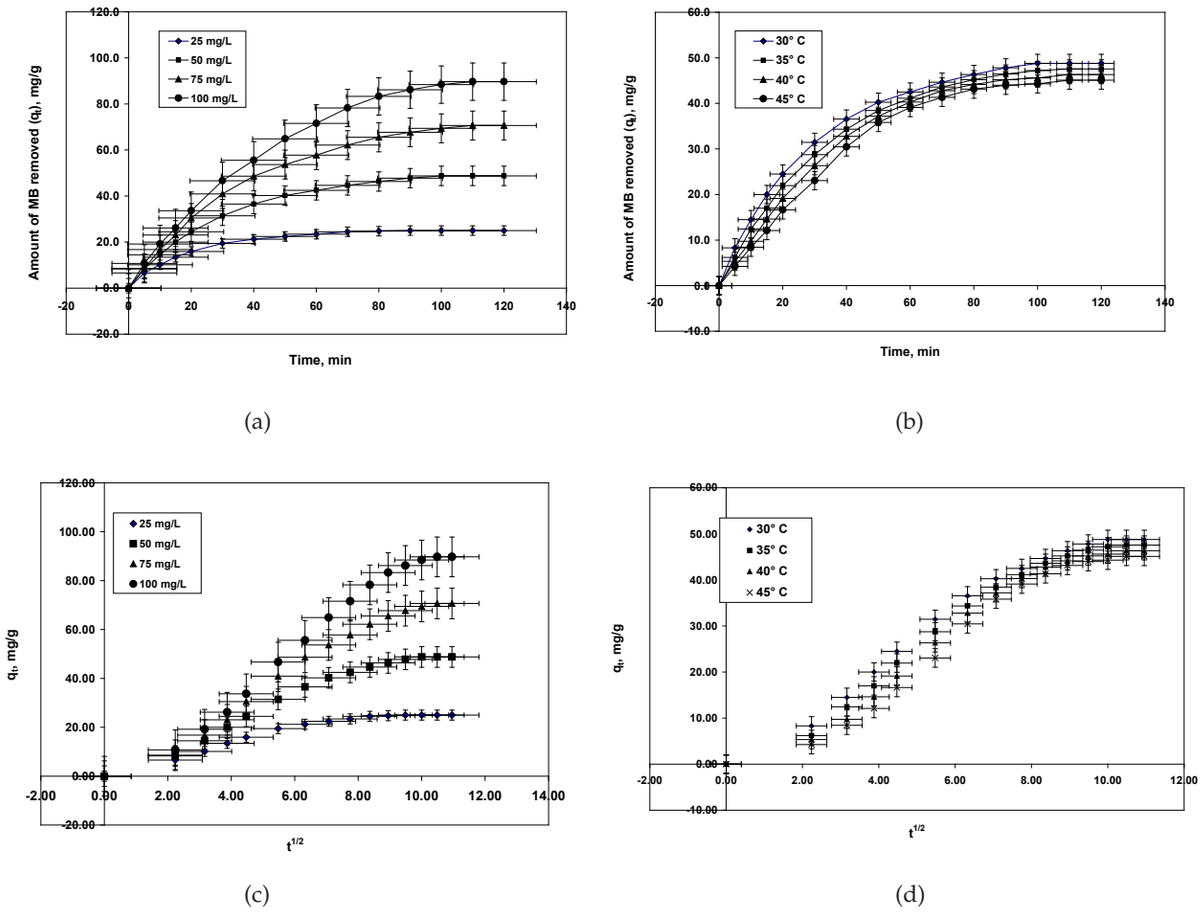

Fig. 6. (a) Effect initial concentration on MB removal, (b) Effect temperature on MB removal, (c) Intra-particle diffusion plot – Initial concentration variation, (d) Intra-particle diffusion plot – Temperature variation.

k_1 is the first-order rate constant (min $^{-1}$), 't' is time (min), k_2 is the rate constant of pseudo second order adsorption (g/mg/min), k_d is the intra particle diffusion rate constant and The initial adsorption rate, h (mg/g/min), as t → 0 can be defined as $h = k_2 q_e^2$.

The adsorption data is analyzed using the above mathematical models and the results are presented in Table 3. The pseudo-first order rate constant (k_1) increased from 0.852 × 10^{-2} to 0.990 × 10^{-2} min^{-1} and the variation is not consistent with respect to concentration increase, the same decreased from 0.852 × 10^{-2} to 0.760 × 10^{-2} min^{-1} on increasing the temperature from 30 to 45° C. The q_e calculated based on the pseudo-first order model show large deviation from the experimentally calculated quantity under the given set of operating conditions. The pseudo-second order rate constant decreased from 0.269 × 10^{-2} to 0.018 × 10^{-2} g/mg/min and 0.070 × 10^{-2} to 0.025 × 10^{-2} g/mg/min on increasing the initial MB concentration and temperature respectively. At higher concentrations, more solutes are available near the boundary layer, the extended boundary layer results in decreased sorption rate. The regression coefficient of pseudo-second order is quite lower than that of pseudo-first order depicts that the adsorption follows pseudo-first order during the beginning of adsorption and in the later stages, it follows pseudo-second order kinetics.

Generally the adsorption mechanism demonstrated in the following four steps. i) creation of a boundary layer around the surface of adsorbent and creating a boundary layer, ii) diffusion of the solute from the boundary layer to the sorbent sites (surface diffusion), iii) solutes from the surface are transported inside the pores (pore diffusion), and iv) formation boning between the solute and sorbet sites (either physical forces of attraction or chemical bonding) [32]. The first step is related to adsorbent and the fourth step is very fast process, therefore these steps are insignificant. The rate controlling step may either be surface diffusion or pore diffusion. The second linear portion of the plot is the gradual adsorption stage where the intra-particle diffusion is the rate limiting. The third portion of the plot depicts the final equilibrium stage where intra-particle diffusion decreased slowly due to the lower concentration of solute in the bulk of the solution [33]. From the results of Intra-particle diffusion plot (Figs. 6c and 6d), the linear portion of the plot did not pass through the origin, which substantiated that the mechanism of MB adsorption by Fe_3O_4@NCB composite is a surface diffusion not the intra-particle pore diffusion [32].

Table 3
Results of kinetic plots

Parameters	Initial dye concentration, mg/L				Temperature, °C		
	25	50	75	100	35	40	45
$q_{eexp.}$ (mg/g)	25.00	48.78	70.70	89.74	47.56	46.34	45.12
Pseudo first order kinetics							
$k_1 \times 10^{-2}$ (min $^{-1}$)	0.967	0.852	0.898	0.990	0.829	0.760	0.760
q_{ecal} (mg/g)	41.39	73.57	101.74	129.00	75.81	76.24	78.14
r^2	0.9017	0.9324	0.9556	0.9759	0.942	0.9269	0.9343
Pseudo second order kinetics							
$k_2 \times 10^{-2}$ (g/mg/min)	0.269	0.070	0.030	0.018	0.051	0.037	0.025
h	2.1720	2.48	2.60	2.83	1.96	1.59	1.27
q_{ecal} (mg/g)	28.41	59.52	93.46	125.00	62.11	65.79	71.43
r^2	0.9831	0.9485	0.8906	0.8452	0.9098	0.8502	0.7489
Intra particle diffusion model							
k_{id} (mg/g/min^{½})	0.2819	0.1839	0.1508	0.1359	0.2875	0.2880	0.2706
r^2	0.9893	0.9672	0.9404	0.9577	0.966	0.9392	0.9215

3.6. Adsorption isotherm

The adsorption isotherm is an expression of rate of change of adsorption with respect to concentration of the adsorbate. It can also represent the nature of distribution of the solute between the liquid and solid phase after the attainment of equilibrium. Several isotherm models have been reported by the past researchers to demonstrate the nature of adsorption. Among the isotherm models, Langmuir [34] and Freundlich [35] isotherm models are the most widely models to describe the adsorption of adsorbate from solution onto the sorbent surface.

3.6.1. Langmuir isotherm

Langmuir isotherm model derived with an assumption that the adsorbent surface is energetically homogeneous and the adsorbate molecules are adsorbed with a single layer and there is no interaction between the adsorbed molecules. The linear form of Langmuir adsorption isotherm is

$$\frac{C_e}{q_e} = \frac{1}{Q_0.b_L} + \frac{C_e}{Q_0} \tag{7}$$

where b_L is the Langmuir constant, C_e is the equilibrium dye concentration in solution, C_0 is the initial concentration (mg/L) and Q_0 is Langmuir monolayer adsorption capacity. The constants Q_0 and b_L can be calculated from the slope and intercept of the plot of "C_e/q_e" *vs* "C_e" (figure not shown) and the results are presented in Table 4. The mono layer adsorption capacity calculated using Langmuir model increases from 192.31 to 277.78 mg/g on increasing the temperature from 30 to 45°C. Owing to the smaller size and large surface area, NCB could adsorb more MB molecules. As given in Table 5, the Q_0 value for the adsorption of MB by Fe_3O_4@ NCB composite is comparable with the value reported in the previous analysis. The Langmuir rate constant b_L decreases from 0.0103 to 0.0067 L/mg on increasing the temperature of the system from 30 to 45° C. The dimensionless factor R_L varied between 0 to 1 (0.469 to 0.937) indicating that the adsorption is favorable under given set of operating conditions using the selected adsorbent-adsorbate system.

Table 4
Results of isotherm plots

Parameters	Temperature °C			
	30	35	40	45
Langmuir isotherm				
Q_0 (mg/g)	192.31	222.22	250.00	277.78
b_L (L/mg)	0.0103	0.0088	0.0077	0.0067
r^2	0.9599	0.9773	0.9768	0.9672
R_L	0.469 to 0.937			
Freundlich isotherm				
n	3.18	2.57	2.22	1.45
k_f (mg$^{1-1/n}$ L$^{1/n}$ g^{-1})	85.82	69.68	56.43	29.28
r^2	0.9797	0.9963	0.9927	0.9895

3.6.2. Freundlich isotherm

The Freundlich [35] adsorption isotherm is one of the oldest mathematical models used to describe the sorption that involves heterogeneous equilibrium. The linearized form of Freundlich model is

$$\log q_e = \log k_f + \frac{1}{n}\log C_e \tag{8}$$

where k_f is related to adsorption capacity and n is related to intensity of adsorption. The Freundlich constants, k_f and n are calculated from the linear plot of "*log* q_e" vs "*log* C_e" (figure not shown) are given in Table 4. The Freundlich parameter related to adsorption capacity (k_f) has decreased

Table 5
Langmuir monolayer adsorption capacity of MB dye on various adsorbents

Adsorbent	Q_0 (mg/g)	Reference
Fe_3O_4 immobilized NCB	192.31 to 277.78	This study
Rattan based activated carbon	294.12	[36]
Biomass based activated carbon	259.25	[32]
Jute fiber carbon	225.64	[37]
Pistachio shell carbon	129.00	[38]
Euphorbia rigida carbon	114.45	[39]
Wood apple rind carbon	40.00	[40]
Citrus fruit peel carbon	25.51	[41]
Hazelnut shell activated carbon	8.82	[42]

from 85.82 to 29.28 $mg^{(1-1/n)}/L^{1/n}/g$ with a raise in temperature from 30 to 45°C. Another parameter n is a measure of adsorption intensity or surface heterogeneity, becoming more heterogeneous as its value gets closer to zero [43]. The results of this study (n = 3.18 to 1.45) substantiates that MB is favorably adsorbed by Fe_3O_4@NCB. On comparing the r^2 value of Langmuir and Freundlich isotherm models, Freundlich model is more appropriate to express the adsorption of MB with high correlation coefficient than Langmuir model.

3.6.3. Thermodynamics of adsorption

Important thermodynamic parameters like free energy (ΔG), enthalpy (ΔH) and entropy (ΔS) changes during the adsorption of MB are evaluated (Table 6) using the following relationships.

$$\Delta G = -RTlnKc \tag{9}$$

$$\ln K_c = \frac{\Delta S}{R} - \frac{\Delta H}{RT} \tag{10}$$

$$lnK_c = {q_e}/{C_e} \tag{11}$$

where R is the universal gas constant (8.314 (J/mole/ K), T is temperature (K), and K_c is the distribution coefficient for the adsorption.

The Gibbs free energy change decreases from –8.578 to –5.882 kJ/mol on increasing the temperature from 30 to 45°C. The negative Gibbs free energy demonstrated that the adsorption is spontaneous under the given set of environmental conditions, whereas the negative free energy decreases on increasing the solution temperature, validated the less spontaneity at higher temperatures. The negative enthalpy change is an indication of heat release (exothermic nature) during the adsorption of MB onto Fe_3O_4@NCB. When the adsorption progresses, the degree of randomness decreases, this is confirmed by the negative entropy change.

Table 6
Thermodynamic parameters for the adsorption of MB onto Fe_3O_4@NCB

Temperature, °C	ΔG, kJ/mol	ΔH, kJ/mol	ΔS J/K/mol
30	–8.578	–60.36	–170.92
35	–7.586		
40	–7.116		
45	–5.882		

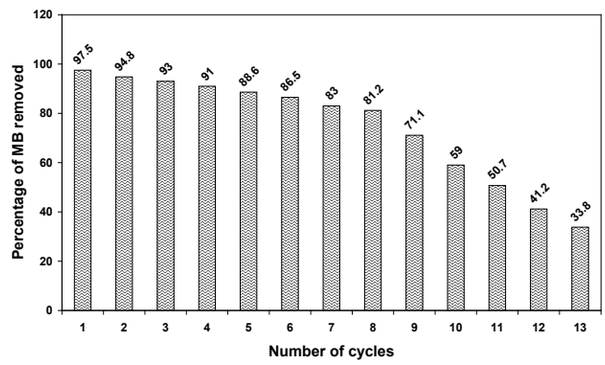

Fig. 7. Reusability studies of regenerated adsorbent.

3.6.4. Adsorbent regeneration studies

Desorption of the adsorbed dye molecules is also performed by varying the eluent pH from 2.0 to 12.0. The desorption of MB dye decreases from 55.72% to 37.33% with increase of pH from 2.0 to 8.0 and there is no considerable change in desorption above pH of 8.0. The desorbed composite can be used for further adsorption studies. The efficiency of the regenerated adsorbent is analyzed for its further use. As observed from Fig. 7, the regenerated adsorbent used up to 8 cycles with more than 80% of dye removal. The dye removal capacity decreases drastically when number of cycles goes above 8. When the number of cycles exceeds 8, the pores of the sorbent are blocked with adsorbate molecules and leads to the drastic reduction of adsorption.

3.7. Column adsorption studies

Packed bed column mode of adsorption has some advantages like continuous operation, easy regeneration, effective contact between the adsorbent and adsorbate. The full scale column at industrial level operations can be designed based on the basis of data collected at laboratory level. Large volume of wastewater can be continuously treated using limited quantity of adsorbent is also an another advantage of the column mode adsorption analysis [44].

3.7.1. Breakthrough curve

The breakthrough curves for the adsorption of MB onto a packed bed column prepared using Fe_3O_4@NCB is shown in Fig. 7. The effect of initial dye concentration of adsorp-

tion performance of MB is studied for a fixed bed height of 5 cm and a flow rate of 10 mL/min. On increasing the initial MB concentration from 25 to 75 mg/L, the MB uptake is increased from 65.61 to 118.78 mg/g. As the concentration of solute goes up, the number of dye molecules competing per unit area of the sorbent surface increases and yields high uptake of dyes per unit weight of the adsorbent. Though, the breakthrough volume decreases on increasing the initial MB concentration, but the quantity of dye removal per unit weight of adsorbent increases. The influence of the flow rate on the adsorption performance is evaluated for a fixed dye concentration of 50 mg/L and the bed depth of 5 cm. As the flow rate increased from 5 to 15 mL/min, the time taken for the exhaustion time also increases. As observed from the Fig. 7, at lower flow rate, the breakthrough curves are gradually raising,on increasing the flow rate from 5 to 15 mL/min, the curves become steeper, indicating quicker breakthrough at higher flow rates. The amount of dye removal per unit mass of Fe_3O_4@NCB decreases drastically from 147.06to 67.87 mg/g, indicating that high flow does not gives enough time for the solute-sorbent interaction when compared with that in the lower flow rate [45]. Lower flow rate makes sure of proper contact between solute and sorbent and thereby yields the maximum efficiency for the adsorbent. The MB removal decreases from 92.76 to 76.92 mg/g on increasing the bed height from 5.0 to 10 cm. Though there is a two fold increase in the sorbent quantity, but the dye removal per unit weight of adsorbent decreases. When the sorbent quantity increased, proportionally the available surface also getting doubled, but the entire sorbent surface is not properly exposed to the solute vicinity and ultimately show decreases in sorption capacity [46].

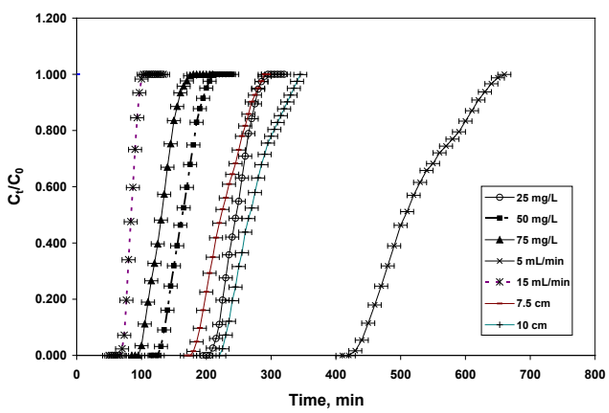

Fig. 8. Breakthrough curves for the column mode adsorption of MB onto Fe_3O_4@NCB.

3.7.2. Thomas model

Thomas model, is one of the earliest model, which describes the kinetics of adsorbent adsorption in a packed bed column [47]. The kinetic model proposed by Thomas has the following form

$$\frac{C_t}{C_0} = \frac{1}{1+\exp\left[k_T\left(q_{0(T)}.m - C_0.v\right)\right]/r} \tag{12}$$

where C_t is effluent dye concentration (mg/L) at time t, C_0 is initial dye concentration (mg/L), k_T is Thomas rate constant, (L/min·mg), $q_{0(T)}$ is maximum dye adsorption capacity (mg/g), m is mass of the adsorbent (g), v is effluent volume (mL) and r is flow rate (ml/min). The value of time, $t = v/r$.

The constants k_T and q_0 were determined from a plot of C_t/C_0 against t for a given set of conditions using non-linear regression analyses (figure not given) are given in Table 7. The Thomas model rate constant show an increasing trend on increasing the concentration of MB and the flow rate and it show a decreasing trend with increasing the bed depth. The adsorption capacity calculated based on this model increased from 72.38 to 151.65 mg/g on increasing the influent concentration from 25 to 75 mg/L and it decreased from 166.74 to 74.32 mg/g and 109.49 to 90.38 mg/g on increasing the flow rate and bed height respectively. The Thomas model fits very poor with the data as observed from the correlation coefficient even it is used in nonlinear regression analysis ($0.8234 < r^2 < 0.9013$).

Table 7
Results column mode adsorption studies of MB

Concentration, mg/L		25	50	75	50	50	50	50
Flow rate, mL/min		10	10	10	5	15	10	10
Bed height, cm		5	5	5	5	5	7.5	10
$q_{0(exp)}$, mg/g		65.61	92.76	118.78	147.06	67.87	85.84	76.92
Break through volume, mL		2900	2050	1750	3250	1500	2850	3400
Thomas model Results	$k_T \times 10^{-3}$, mL/min/mg	0.960	0.420	1.470	0.160	1.470	0.340	0.260
	$q_{0(T)}$, mg/g	72.38	109.49	151.65	166.74	74.32	100.17	90.38
	r^2	0.8234	0.9013	0.8735	0.8718	0.8509	0.8293	0.8255
	Sd	1.33	3.28	6.45	3.86	1.26	2.81	2.64
Yoon Nelson Model results	$k_{(YN)}$, L/min	0.09	0.11	0.23	0.03	0.23	0.06	0.05
	τ, min	245.74	163.62	129.89	524.11	84.36	228.69	273.53
	$q_{0(YN)}$, mg/g	55.60	74.04	88.16	118.58	57.25	68.88	61.88
	r^2	0.9669	0.979	0.9716	0.8718	0.8509	0.8293	0.8255
	Sd	1.96	3.67	6.00	5.59	2.08	3.33	2.95

3.7.3. Yoon-Nelson model

Yoon and Nelson (1984) have proposed a less complicated model to represent the breakthrough of gases onto activated charcoal [48]. The model is proposed based on the assumption that "the rate of decrease in the probability of adsorption for each adsorbate molecule is proportional to the probability of adsorbate adsorption and the probability of adsorbate breakthrough on the adsorbent". The linear form of Yoon-Nelson model is

$$\ln\left(\frac{C_t}{C_0 - C_t}\right) = k_{YN}.t - \tau.k_{YN} \tag{13}$$

where k_{YN} is Yoon-Nelson rate constant, t is the time required for 50% of adsorbate breakthrough and t is the sampling time. A plot of $\ln\left(\frac{C_t}{C_0 - C_t}\right)$ vs. t gives a straight line with a slope of k_{YN} and intercept of $-t.k_{YN}$.

Based on Yoon-Nelson model, the amount of dye being adsorbed in a fixed bed is half of the total dye entering the adsorption bed within 2t period [49]. For a given bed:

$$q_{0YN} = \frac{q_{(total)}}{m} = \frac{\frac{1}{2}C_0[(r/1000)\times 2\tau]}{m} = \frac{C_0.r.\tau}{1000m} \tag{14}$$

From this equation, the adsorption capacity, $q_{0(YN)}$ varies as a function of inlet dye concentration (C_0), Flow rate (r), weight of adsorbent (m) and 50% breakthrough time. The Yoon-Nelson rate constant k_{YN} increases on increasing the concentration of MB as well as the flow rate and decreases on increasing the bed depth. At high concentration and high flow rate, the number of dye molecules crossing through a particular sorbent surface is more, hence show a higher rate. At higher bed height, the adsorbate molecules has to travel a long distance through the column and also the solute/sorbent ratio is less which results in the reduced rate of adsorption. The time required for 50% breakthrough t decreases from 245.74 to 129.89 min and 524.11 to 84.36 min on increasing the concentration and flow rate respectively. Increase of bed depth increases t from 163.62 to 273.53 min. Expression of column kinetics using a mathematical model is a highly complicated process, the Thomas model though has low r^2 but the standard deviation of the adsorption capacity with that of experimental value is less. On contrary, Yoon-Nelson model though the r^2 is good but the calculated adsorption capacity show large deviation when compared with the Thomas model.

4. Conclusion

Synthesis of nano sized carbon balls (NCB) with a uniform size of <100 nm are successfully synthesized from *Madhucalongifolia* oil as a precursor oil. The multi-metal catalyst derived from *Alternanthera sessilis* stem ash helps the formation of strings of carbon balls. The magnetically immobilized NCB has great potential for the removal of methylene blue dye under batch and column mode of adsorption. SEM and XRD studies revealed the structure of NCB and its immobilization with Fe_3O_4. Kinetic studies proved that the composite follows pseudo-first order during the beginning of adsorption and later it deviates to pseudo-second order. Freundlich adsorption isotherm is more appropriate for the demonstration of this adsorption system. Exothermic and spontaneous nature of adsorption is proved by the thermodynamic studies. The composite column is successfully tested for the removal of MB and this study proved that the synthesized composite is a good adsorbent for textile dyes.

Acknowledgment

The author Dr. P. Sivakumar thank, Tamil Nadu State Council for Higher Education, Tamil Nadu (TANSCHE), India for the financial assistance under "Minor Research Project (Science & Humanities) Scheme for the year 2016–2017 (Project Ref.:D.O.Rc. No. 756/2016A, Dt. 27.03.2017)".

References

[1] X. Li, W.C. Cao, Y.G. Liu, G.M. Zeng, W. Zeng, L. Qin, T.T. Li, The property variation of magnetic mesoporous carbon modified by aminated hollow magnetic nano spheres: Synthesis, characteristic and sorption, ACS Sustain. Chem. Eng., 5 (2017) 179–88.

[2] S.M. Twanga, M.A.A Zainia, L.M. Salleha, M.A.C. Yunusa, M. Naushad, Potassium hydroxide-treated palm kernel shell sorbents for the efficient removal of methyl violet dye, Desal. Water Treat., 84 (2017) 262–270.

[3] E. Daneshvar, A. Vazirzadeh, A. Niazi, M. Kousha, M. Naushad, A. Bhatnagar, Desorption of methylene blue dye from brown macroalga: Effects of operating parameters, isotherm study and kinetic modeling, J. Cleaner Prod., 152 (2017) 443–453.

[4] G. Sharma, M. Naushad, A. Kumar, S. Rana, S. Sharma, A. Bhatnagar, F.J. Stadler, A.A. Ghfar, M.R. Khan, Efficient removal of coomassie brilliant blue R-250 dye using starch/poly (alginic acid-cl-acrylamide) nano hydrogel, Pro. Safety Environ. Protect., 109 (2017) 301–310.

[5] G. Sharma, A. Kumar, M. Naushad, A. Kumar, A.H. Al-Muhtaseb, P. Dhiman, A.A. Ghfa, F.J. Stadler, M.R. Khan, Photo remediation of toxic dye from aqueous environment using mono metallic and bimetallic quantum dots based nano composites, J. Cleaner Prod. (Accepted), (2017) DOI: 10.1016/j.jclepro.2017.11.122.

[6] A. Ampoumogli, T. Steriotis, P. Trikalitis, E.G. Bardaji, M. Fichtner, A. Stubos, G. Charalambopoulou, Synthesis and characterisation of a mesoporous carbon/calcium borohydride nano composite for hydrogen storage, Int. J. Hydrogen Energy, 37 (2012) 16631–16635.

[7] J. Marie, R. Chenitz, M. Chatenet, S. Berthon-Fabry, N. Cornet, P. Achard, Highly porous PEM fuel cell cathodes based on low density carbon aerogels as Pt- support: Experimental study of the mass-transport losses, J. Power Sources, 190 (2009) 423–434.

[8] A.A. Alqadami, M. Naushad, M.A. Abdalla, M.R. Khan, Z.A. Alothman, Adsorptive removal of toxic dye using Fe_3O_4 -TSC nano composite: Equilibrium, kinetic and thermodynamic studies, J. Chem. Eng. Data (in press), (2016) DOI: 10.1021/acs.jced.8b00024.

[9] M. Naushad, T. Ahamad, B.M. Al-Maswari, A.A. Alqadami, S.M. Alshehri, Nickel ferrite bearing nitrogen-doped mesoporous carbon as efficient adsorbent for the removal of highly toxic metal ion from aqueous medium, Chem. Engg. J. (Accepted) (2017) DOI:http://dx.doi.org/10.1016/j.cej.2017.08.079.

[10] Y. Fan, P.F. Liu, Z.Y. Huang, T.W. Jiang, K.L. Yao, R. Han, Porous hollow carbon spheres for electrode material of super capacitors and support material of dendritic Pt electro catalyst, J. Power Sources, 280 (2015) 30–38.

[11] B. Murugesan, A. Sivakumar, A. Loganathan, P. Sivakumar, Synthesis and photo catalytic studies of lanthanum oxide doped nano carbon hollow spheres, J. Taiwan Inst. Chem. Eng., 71 (2017) 364–72.
[12] V.V. Kovalevski, A.N. Safronov, Pyrolysis of hollow carbons on melted catalyst, Carbon, 36 (1998) 963–968.
[13] M. Inagaki, Carbon materials structure, texture and intercalation, Solid State Ionics, 86 (1996) 833–839.
[14] Trifed, "Product profile, Mahuwa, Ministry of Tribal Affairs, Government of India". Trifed.nic.in. Retrieved 2013-11–21.
[15] S.H. Kim, G.W. Mulholland, M.R. Zachariah, Density measurement of size selected multi walled carbon nano tubes by mobility-mass characterization, Carbon, 47 (2009) 1297–1302.
[16] Y.Z. Jin, C. Gao, W.K. Hsu, Y. Zhu, A. Huczko, M. Bystrzejewski, M. Roe, C.Y. Lee, S. Acquah, H. Kroto, D.R.M. Walton, Large scale synthesis and characterization of carbon spheres prepared by direct pyrolysis of hydrocarbons, Carbon, 43 (2005) 1944–1953.
[17] L. Wan, Q. Zhao, P. Zhao, B. He, T. Jiang, Q. Zhang, S. Wang, Versatile hybrid polyethyleneimine mesoporous carbon nano particles for targeted delivery, Carbon, 79 (2014) 123–134.
[18] P.N. Palanisamy, P. Sivakumar, Kinetic and isotherm studies of the adsorption of Acid Blue 92 using a low-cost non-conventional activated carbon, Desalination, 249 (2009) 388–397.
[19] S.H. Ng, J. Wang, Z.P. Guo, J. Chen, G.X. Wang, H.K. Liu, Single wall carbon nano tube paper as anode for lithium-ion battery, Electrochim. Acta, 51 (2005) 23–28.
[20] A. Nieto-Marquez, I. Espartero, J.C. Lazo, A. Romero, J.L. Valverde, Direct synthesis of carbon and nitrogen-carbon nano spheres from aromatic hydrocarbons, Chem. Eng. J., 153 (2009) 211–216.
[21] Y. Jin, C. Zhao, Y. Lin, D. Wang, L. Chen, C. Shen, Fe-based metal-organic framework and Its derivatives for reversible, J. Mater. Sci. Technol., 33(8) (2017) 768–774.
[22] C. Shuai, X. Yuelong, Z. Yiyang, Z. Feng, M. Yurong, Z. Henghui, Q. Limin, Branched CNT@SnO_2 nanorods@carbon hierarchical hetero structures for lithium ion batteries with high reversibility and rate capability, J. Mater. Chem. A, 2 (2014) 15582–15589.
[23] M.S. Kim, N.M. Rodriguez, R.T.K. Baker, The interaction of hydrocarbons with coppernickel and nickel in the formation of carbon filaments, J. Catal., 131 (1991) 60–73.
[24] S. Tian, L. Lu, J.M. Labavitch, S.M. Webb, X. Yang, P.H. Brown, Z. He, Spatial imaging of Zn and other elements in Huang long bing affected grape-fruit by synchrotron-based micro X-ray fluorescence investigation, J. Exp. Bot., 65 (2014) 953–964.
[25] N. Gopal, M. Asaithambi, P. Sivakumar, V. Sivakumar, Adsorption studies of a direct dye using polyaniline coated activated carbon prepared from Prosopis juliflora, J. Water Proc. Eng., 2 (2014) 87–95.
[26] J.U. Keller, R. Staudt, Gas adsorption equilibria, experimental methods and adsorptive isotherms. 2005. Springer. Boston. MA
[27] P. Zhang, I. Lo, D. O'Connor, S. Pehkonen, H. Cheng, D. Hou, High efficiency removal of methylene blue using SDS surface-modified $ZnFe_2O_4$ nano particles, J. Colloid. Interface Sci., 508 (2017) 39–48.
[28] Y. Bao, G. Zhang, Study of adsorption characteristics of methylene blue onto activated carbon made by salixpsammophila, Energy Procedia, 16 (2012) 1141–1146.
[29] S. Langergen, B.K. Svenska, Zurtheorie der sogenanntenadsoptiongeloesterstoffe. VeteruskapsakadHandlingar, 24 (1898) 1–39.
[30] Y.S. Ho, G. Mckay, Pseudo-second order model for sorption processes, Proc. Biochem., 34 (1999) 451–465.
[31] W.J. Weber, J.C. Morris, Kinetics of adsorption on carbon from solution, J. Sanitary Eng. Division. Am. Soc. Civil Eng., 89 (1963) 31–60.
[32] S.K. Theydan, M.J. Ahmed, Adsorption of methylene blue onto biomass-based activated carbon by $FeCl_3$ activation: Equilibrium, kinetics, and thermodynamic studies, J. Anal. App. Pyrolysis, 97 (2012) 116–122.
[33] F.C. Wu, R.L. Tseng, R.S. Juang, Comparisons of porous and adsorption properties of carbons activated by steam and KOH, J. Colloid Interf. Sci., 283 (2005) 49–56.
[34] I. Langmuir, The adsorption of gases on plane surfaces of glass, mica and platinum, J. Am. Chem. Soc., 40 (1918) 1361–1403.
[35] H.M.F. Freundlich, Uber die adsorption in losungen, Z. Phys. Chem., 57 (1906) 385–470.
[36] B.H. Hameed, A.L. Ahmad, K.N.A. Latiff, Adsorption of basic dye (methylene blue) onto activated carbon prepared from rattan sawdust, Dyes Pigments, 75 (2007) 143–149.
[37] S. Senthilkumaar, P.R. Varadarajan, K. Porkodi, C.V. Subbhuraam, Adsorption of methylene blue onto jute fiber carbon: kinetics and equilibrium studies, J. Colloid. Interface Sci., 284 (2005) 78–82.
[38] A.A. Attia, B.S. Girgas, S.A. Khedr, Capacity of activated carbon derived from pistachio shells by H_3PO_4 in the removal of dyes and phenolics, J. Chem. Technol. Biotechnol., 78 (2003) 611–619.
[39] O. Cercel, A. Ozcan, A.S. Ozcan, H.F. Gercel, Preparation of activated carbon from renewable bio-plant of Eupharbiarigida by H_2SO_4 activation and its adsorption behavior in aqueous solutions, Appl. Surf. Sci., 253 (2007) 4843–4852.
[40] R. Malarvizhi, Y.S. Ho, The influence of pH and the structure of the dye molecules on adsorption isotherms modeling using activate carbon, Desalination, 264 (2010) 97–101.
[41] S. Dutta, A. Bhattacharyya, A. Ganguly, S. Gupta, S. Basu, Application of response surface methodology for preparation of low-cost adsorbent from citrus fruit peel and for removal of methylene blue, Desalination, 275 (2011) 26–36.
[42] A. Aygun, X.S. Yenisoy-Karakas, I. Duman, Production of granular activated carbon from fruit stones and nutshells and evaluation of their physical, chemical and adsorption properties, Microporous. Mesoporous. Mater., 66 (2003) 189–195.
[43] F. Haghseresht, G. Lu, Adsorption characteristics of phenolic compounds onto coal-reject-derived adsorbents, Energy Fuels, 12 (1998) 1100–1107.
[44] N. Gopal, M. Asaithambi, P. Sivakumar, V. Sivakumar, Continuous fixed bed adsorption studies of Rhodamine-B dye using polymer bound adsorbent, Indian J. Chem. Technol., 23 (2016) 53–58.
[45] P. Sivakumar, P.N. Palanisamy, Packed bed column studies for the removal of Acid blue 92 and Basic red 29 using non-conventional adsorbent, Indian J. Chem. Technol., 16 (2009) 301–307
[46] K. Vijayaraghavan, J. Jegan, K. Palanivelu, M. Velan, Removal of nickel(II) ions from aqueous solution using crab shell particles in a packed bed up-flow column, J. Hazard. Mater., 113 (2004) 223–230.
[47] H.C. Thomas, Heterogeneous ion exchange in a flowing system, J. Am. Chem. Soc., 66 (1944) 1664–1666.
[48] Y.H. Yoon, J.H. Nelson, Application of gas adsorption kinetics. I. A theoretical model for respirator cartridge service life, Am. Ind. Hyg. Assoc. J., 45 (1984) 509–516.
[49] Z. Zulfadhly, M.D. Mashitah, S. Bhatia, Heavy metals removal in fixed-bed column by the macro fungus Pycnoporussanguineus, Environ. Pollut., 112 (2001) 463–470.